Engineering 7 (2021) 1306–1312

Contents lists available at ScienceDirect

Engineering

journal homepage: www.elsevier.com/locate/eng

Research
Hydrogen Energy—Article

Bimetallic Oxyhydroxide as a High-Performance Water Oxidation Electrocatalyst under Industry-Relevant Conditions

Jiaxin Yuan [a], Xiaodi Cheng [a], Chaojun Lei [a], Bin Yang [a], Zhongjian Li [a], Kun Luo [c], K.H. Koko Lam [d], Lecheng Lei [a], Yang Hou [a,b,*], Kostya Ken Ostrikov [e]

[a] Key Laboratory of Biomass Chemical Engineering of the Ministry of Education, College of Chemical and Biological Engineering, Zhejiang University, Hangzhou 310027, China
[b] Institute of Zhejiang University–Quzhou, Quzhou 324000, China
[c] State Key Laboratory of Clean Energy Utilization, Zhejiang University, Hangzhou 310027, China
[d] Department of Electrical Engineering, The Hong Kong Polytechnic University, Hong Kong 999077, China
[e] School of Chemistry, Physics, and Mechanical Engineering, Queensland University of Technology, Brisbane, QLD 4001, Australia

ARTICLE INFO

Article history:
Received 9 July 2019
Revised 28 October 2019
Accepted 2 January 2020
Available online 11 June 2021

Keywords:
Bimetallic oxyhydroxide
3D hybrid
Electrocatalysis
Oxygen evolution reaction
High current density

ABSTRACT

Developing high-performing oxygen evolution reaction (OER) electrocatalysts under high-current operation conditions is critical for future commercial applications of alkaline water electrolysis for clean energy generation. Herein, we prepared a three-dimensional (3D) bimetallic oxyhydroxide hybrid grown on a Ni foam (NiFeOOH/NF) prepared by immersing Ni foam (NF) into $Fe(NO_3)_3$ solution. In this unique 3D structure, the NiFeOOH/NF hybrid was composed of crystalline $Ni(OH)_2$ and amorphous FeOOH evenly grown on the NF surface. As a bimetallic oxyhydroxide electrocatalyst, the NiFeOOH/NF hybrid exhibited excellent catalytic activity, surpassing not only the other reported Ni–Fe based electrocatalysts, but also the commercial Ir/C catalyst. *In situ* electrochemical Raman spectroscopy demonstrated the active FeOOH and NiOOH phases involved in the OER process. Profiting from the synergy of Fe and Ni catalytic sites, the NiFeOOH/NF hybrid delivered an outstanding OER performance under challenging industrial conditions in a 10.0 mol·L^{-1} KOH electrolyte at 80 °C, requiring potentials as small as 1.47 and 1.51 V to achieve the super-high catalytic current densities of 100 and 500 mA·cm^{-2}, respectively.

1. Introduction

In a context of the development of global power and environmental concerns, electrocatalytic water splitting is a promising renewable and clean energy technology that can convert a large amount of water into hydrogen and oxygen [1,2]. Electrochemical water splitting involves two half reactions; of these, the oxygen evolution reaction (OER) is a four-step electron-transfer reaction [3] that requires a higher overpotential and thus greatly reduces the overall reaction rate, acting as a reaction bottleneck for hydrogen production from electrolyzed water [4,5]. At present, the most efficient OER electrocatalysts are mainly based on noble metal compounds (e.g., RuO_2, IrO_2, and Ir/C) because of their high catalytic activity and high level of stability [6,7]. However, the shortage of these expensive metal compounds limits their wide application [8]. Therefore, it is of great significance to explore highly competent, stable, and low-cost OER electrocatalysts such as transition-metal (e.g., iron (Fe), cobalt (Co), and nickel (Ni)) oxides [9,10], nitrides [11], borides [12], carbides [13], oxyhydroxides [14], hydroxides [15], chalcogenides [16,17], and phosphorus compounds [18,19]. Among these, Ni-based OER electrocatalysts not only are low in cost and abundant in reserves, but also exhibit good stability for the OER process in alkaline media [20]. However, the poor electronic conductivity of Ni-based OER materials makes their electrocatalytic performance far from satisfactory.

Recently, binary metal-based catalysts with high intrinsic catalytic activity have been employed as efficient OER catalysts for water splitting, instead of single metal-based catalysts [21], due to their enhanced intrinsic catalytic properties [22]. Among the various metals that have been introduced in this area, metallic Fe has become a widely studied material by virtue of its remarkable catalytic performance, strong chemical stability, and low cost [23]. In addition, although a certain amount of progress has been made in the development of highly efficient OER catalysts operating under the conditions of real-world industrial applications

* Corresponding author.
E-mail address: yhou@zju.edu.cn (Y. Hou).

https://doi.org/10.1016/j.eng.2020.01.018

(10.0 mol·L^{-1} KOH, 80 °C, and up to 500 mA·cm^{-2}), their overall electrocatalytic efficiency remains poor and their synthetic methods are still complicated.

Herein, we prepared a novel three-dimensional (3D) bimetallic oxyhydroxide hybrid consisting of crystalline $Ni(OH)_2$ and amorphous FeOOH grown on a Ni foam (NF) during a displacement reaction at room temperature, in which the NF was etched by $Fe(NO_3)_3$ solution. Due to the synergy of the Fe and Ni catalytic sites, the NiFeOOH/NF hybrid exhibited admirable OER activity and stability in alkaline media, reaching the commercially required current densities of 500 and 1000 mA·cm^{-2} at 1.51 and 1.55 V, respectively. Importantly, these measured potentials are among the lowest when compared with other reported Ni–Fe based electrocatalysts, as well as the benchmark Ir/C catalyst [24]. The FeOOH and NiOOH phases were specifically OER-active of the NiFeOOH/NF hybrid, as discovered by *in situ* electrochemical Raman spectroscopy. Furthermore, the NiFeOOH/NF hybrid was found to have superior OER activity and corrosion resistance in a widely adopted electrolyte in commercial water–alkali electrolyzers—namely, 10.0 mol·L^{-1} KOH electrolyte at 80 °C.

2. Material and methods

2.1. Catalyst preparation

To prepare the (NiFeOOH)/NF, commercial NF was immersed in turn in 1.0 mol·L^{-1} HCl, acetone, ethanol, and then deionized water for 10 min each in an ultrasonic machine. After these treatments, three pieces of NF were dipped into 0.2 mol·L^{-1} of $Fe(NO_3)_3$ solution with mechanical shaking for 3 min and then dehydrated at room temperature. The loading amount of NiFeOOH catalyst was approximately 10 mg·cm^{-2}.

2.2. Physical characterization

The morphologies and microstructures of the samples were surveyed by field-emission scanning electron microscopy (FESEM, Supra 55, Hitachi, Japan) and transmission electron microscopy (TEM) measurements performed on a JEM-2100 electron microscope (JEM-2100, 200 kV, JEOL, Japan) with an expediting voltage of 200 kV. Raman spectra were recorded on a Raman scattering spectroscopy system (LabRAM HR Evolution, Horiba Jobin Yvon, France) with excitation by a diode laser (532 nm) in the backscattering geometry. Rigaku D/Max 2550/PC (Rigaku Corporation, Japan) was used to obtain the X-ray diffraction (XRD) patterns, and X-ray photoelectron spectroscopy (XPS, ESCALAB 250Xi, Thermo Fisher Scientific Inc., USA) was performed using Al Kα radiation.

2.3. Electrochemical measurements

Electrochemical tests were performed in a three-electrode cell using 1.0 mol·L^{-1} KOH as the electrolyte. The NiFeOOH/NF sample, a carbon rod, and an Ag/AgCl electrode acted as the working, counter, and reference electrodes, respectively. The mechanical robustness and stability were studied through multiple-current steps, multiple-potential steps, and amperometric current–time measurements. After the cyclic voltammetry (CV) cycles were stabilized, electrochemical measurements were performed. Linear sweep voltammetry (LSV) was used to acquire the OER catalytic activity with a scan rate of 5 mV·s^{-1}. To ascertain the double-layer capacitance (C_{dl}), CV scans between 0.21 and 0.31 V (vs Ag/AgCl) were conducted at 20, 40, 60, 80, and 100 mV·s^{-1}. The potentials versus reversible hydrogen electrode (RHE) in 1.0 mol·L^{-1} at 25 °C were calculated through the original Nernst equation:

$$E_{RHE} = E_{Ag/AgCl} + 0.0591\,pH + 0.098\,V$$

3. Results and discussion

A simple immersion and shocking process was employed to synthesize the 3D NiFeOOH/NF hybrid. The 3D NF sample was introduced into the $Fe(NO_3)_3$ solution, followed by mechanical shaking for 3 min. NF and Fe^{3+} undergo a redox reaction to form the NiFeOOH/NF hybrid, which consists of crystalline $Ni(OH)_2$ and amorphous FeOOH [25]. We systematically identified the effects of different $Fe(NO_3)_3$ concentrations to achieve the highest OER activity; the optimized concentration was 0.2 mol·L^{-1} (Appendix A Fig. S1). A low-resolution FESEM image of the NiFeOOH/NF material showed that the NiFeOOH hybrid was uniformly grown on the 3D NF sample (Figs. 1(a) and (b)). Moreover, elemental mapping of the NiFeOOH/NF hybrid (Fig. 1(c) and Appendix A Fig. S2) showed that the Fe, Ni, and oxygen (O) elements were homogeneously distributed over the 3D surface area. The NiFeOOH/NF exhibited interplanar spacings of 0.460 and 0.270 nm, which were ascribed to the (001) and (100) planes of $Ni(OH)_2$ in high-resolution TEM (HRTEM) images (Fig. 1(d) and Appendix A Fig. S3). The corresponding selected-area electron diffraction (SAED) pattern affirmed that the $Ni(OH)_2$ in the NiFeOOH/NF hybrid was crystalline (Fig. 1(e)). The XRD pattern of the NiFeOOH/NF hybrid showed the existence of crystalline $Ni(OH)_2$ (Joint Committee on Powder Diffraction Standards (JCPDS) 14–0117) and the Ni substrate (JCPDS 70–0989) (Fig. 1(f)) [26]. No characteristic diffraction peaks of FeOOH species were observed due to its amorphous structural features and high dispersion on the surface of NF [27]. The presence of amorphous FeOOH film in the NiFeOOH/NF hybrid was further revealed by Raman spectroscopy (see below).

Given these findings, it can be concluded that the NiFeOOH/NF hybrid was composed of $Ni(OH)_2$ with moderate crystallinity and amorphous FeOOH. The cohabiting of the O, Fe, and Ni elements was analyzed by XPS measurements (Appendix A Fig. S4). The high-revolution Fe 2p signals of the NiFeOOH/NF hybrid were located at 711.8 and 724.6 eV, which are related to the Fe $2p_{3/2}$ and Fe $2p_{1/2}$ states, respectively, with two satellite peaks at 717.1 and 732.2 eV (Fig. 1(g)) [14,28–30]. The high-revolution Ni 2p XPS spectrum showed the Ni $2p_{3/2}$ and Ni $2p_{1/2}$ peaks centered at approximately 855.9 and 873.5 eV, respectively, which were attributed to Ni^{2+} (Fig. 1(h)) [31–34]. The high-revolution O 1s XPS spectrum of the NiFeOOH/NF hybrid exhibited three peaks located at 529.4, 531.4, and 532.8 eV, which were assigned to the Fe–O and Fe–OH bonds in the FeOOH structure and to the H–O–H bonds in the H_2O species, respectively (Fig. 1(i)) [24,35].

The OER electrocatalytic activity of the NiFeOOH/NF hybrid was examined using a three-electrode system in 1.0 mol·L^{-1} KOH solution. For comparison, commercial Ir/C/NF, NF, and carbon paper (CP) immersed in $Fe(NO_3)_3$ solution ($Fe(NO_3)_3$/CP) were also studied (Fig. 2(a)). In contrast to the control samples, the NiFeOOH/NF hybrid exhibited an extraordinary OER activity with low potentials of 1.46, 1.51, and 1.55 V to achieve 100, 500, and 1000 mA·cm^{-2}, respectively. It is noteworthy that the NiFeOOH/NF hybrid can supply a current density of up to 1400 mA·cm^{-2} at a small potential of 1.57 V. This extraordinary catalytic behavior means that the NiFeOOH/NF hybrid satisfies the commercial criteria of OER electrocatalysis under basic electrolyte conditions. The NiFeOOH/NF hybrid clearly exhibited a much smaller potential of 1.51 V in comparison with $Fe(NO_3)_3$/CP (1.71 V) at 500 mA·cm^{-2} (Fig. 2(b)). This potential of the NiFeOOH/NF hybrid is much lower than that of most reported Ni–Fe-based electrocatalysts, as well as that of commercial Ir/C/NF, which is 1.59 V at 500 mA·cm^{-2}.

The reaction kinetic activity of the NiFeOOH/NF hybrid was further evaluated using its Tafel slope; Fig. 2(c) and Fig. S5 in Appendix A exhibit the Tafel slope of 58.4 mV·dec^{-1}, which is lower than

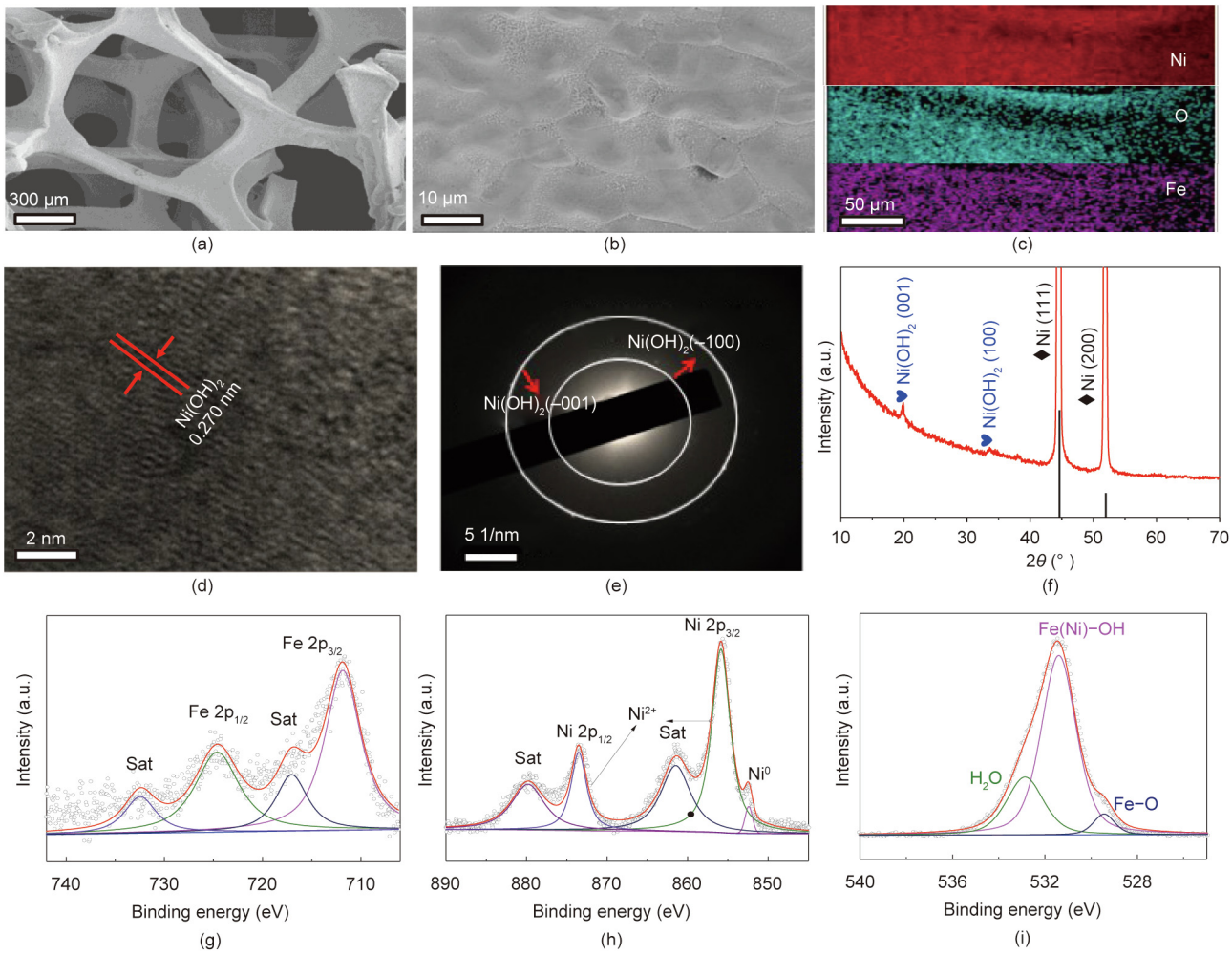

Fig. 1. (a, b) FESEM images of NiFeOOH/NF. (c) Corresponding elemental mapping images of Ni, O, and Fe elements in NiFeOOH/NF. (d) HRTEM image of NiFeOOH/NF. (e) SAED pattern of NiFeOOH/NF. (f) XRD pattern of NiFeOOH/NF. XPS spectra of (g) Fe 2p, (h) Ni 2p, and (i) O 1s for NiFeOOH/NF. Sat: satellite peak.

the 60.9 mV·dec^{-1} Tafel slope of Ir/C/NF and the 96.3 mV·dec^{-1} Tafel slope of $Fe(NO_3)_3$/CP. This finding implies that the NiFeOOH/NF hybrid possesses fast OER kinetics and inherent outstanding activity toward the OER process. It is notable that the matching Tafel slope and the potential of the NiFeOOH/NF hybrid are almost at the minimum at 100 mA·cm^{-2}. In addition, the Tafel slope is low in comparison with those of previously reported Ni–Fe-based electrocatalysts (Fig. 2(d) and Appendix A Table S1). These results further demonstrate the outstanding OER performance of the NiFeOOH/NF hybrid. Fig. 2(e) presents the multistep chronopotentiometric curve acquired for the NiFeOOH/NF hybrid under alkaline conditions; with a varying current density from 200 to 1200 mA·cm^{-2}, the voltage remains constant for the remaining 200 s. These factors confirm the exceptional mechanical robustness and excellent mass transport of the NiFeOOH/NF hybrid [36,37].

Electrochemical durability is a key performance indicator of electrocatalysts. In cyclic voltammogram testing, the polarization curve of the NiFeOOH/NF hybrid after the 500-cycle test remained almost unchanged when compared with the initial one (Fig. 2(f)), indicating the high electrochemical stability of the NiFeOOH/NF hybrid [38]. A chronopotentiometry test over 10 h of continuous reaction further demonstrated the long-term durability of the NiFeOOH/NF hybrid. Notably, the NiFeOOH/NF hybrid also exhibited good stability under 1000 mA·cm^{-2} at 2.0 V after chronoamperometry testing for over 10 h (Fig. 2(f) and Appendix A Fig. S6).

To further explore the effect of sample preparation conditions on the OER performance, mechanical shocks were applied for different time intervals during the synthesis process. Electrochemical tests of the NiFeOOH/NF hybrids prepared using mechanical shocks applied with different time intervals were performed. The NiFeOOH/NF hybrid exhibited a larger current density and smaller onset potential than the hybrid samples prepared with the mechanical shocking time intervals of 0.5, 1.0, and 5.0 min (Appendix A Fig. S7). Similarly, the NiFeOOH/NF (3 min) hybrid exhibited the greatest electrochemical double-layer capacitance (C_{dl}) value of 14.61 mF·cm^{-2} in comparison with the other control NiFeOOH/NF (0.5, 1.0, and 5.0 min) hybrid samples. These results suggest that the NiFeOOH/NF hybrid featured the most highly exposed active surface areas among all the studied samples (Fig. 3(a) and Appendix A Fig. S8) [39]. Furthermore, electrochemical impedance spectroscopy (EIS) of the NiFeOOH/NF hybrid revealed the minimum charge transfer resistance and the fastest electron-transfer ability among all the studied NiFeOOH/NF hybrid samples (Fig. 3(b)). In the inset of Fig. 3(b), where the R_s is the solution resistance, constant-phase element (CPE1) is related to the double-layer capacitance and R_{ct} is charge-transfer resistance. Importantly, this simple immersion and shocking method were further developed to synthesize a sequence of $Co(NO_3)_2$/NF, $Cu(NO_3)_2$/NF, $Mg(NO_3)_2$/NF, $Ni(NO_3)_2$/NF, and $Zn(NO_3)_2$/NF compounds. To further identify the effect of the possible synergy between the different metals on OER efficiency, a battery of electrochemical tests was performed. The

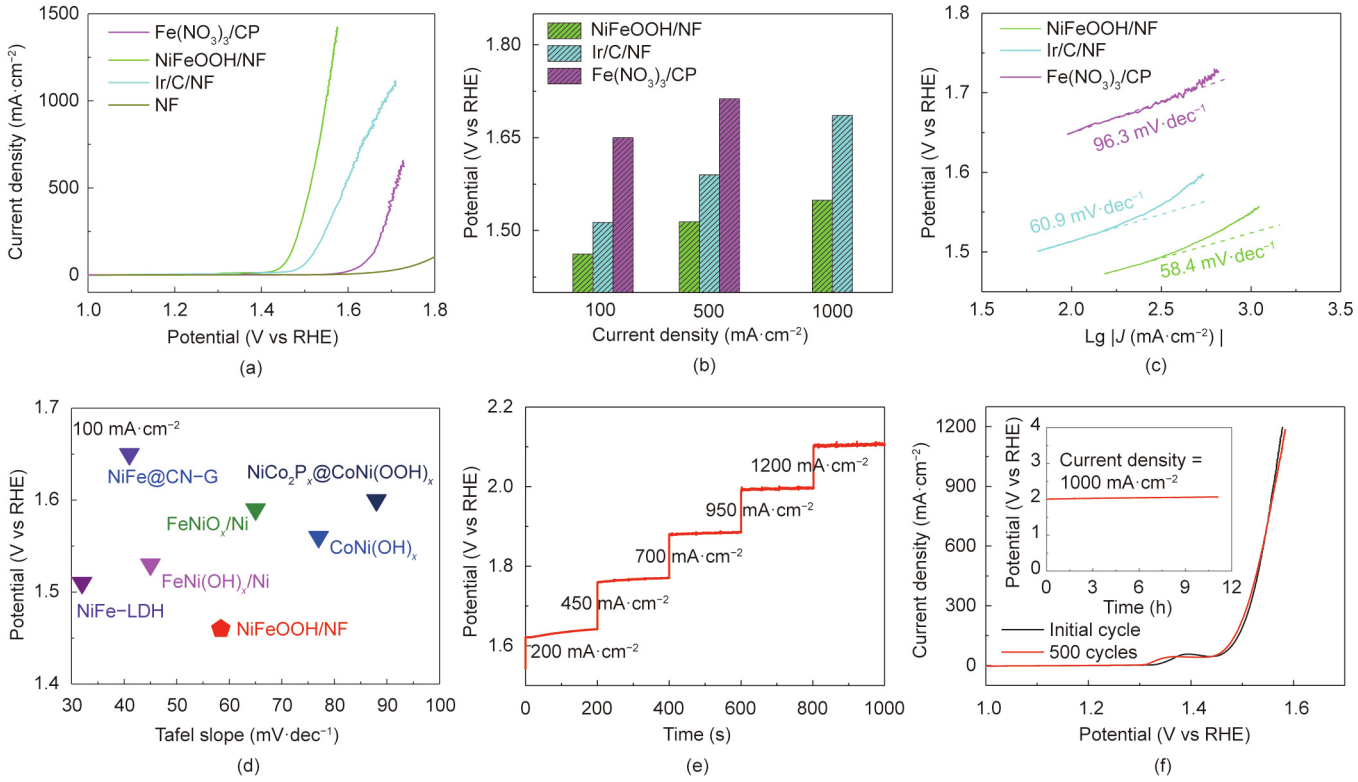

Fig. 2. (a) OER LSV curves of $Fe(NO_3)_3$/CP, NiFeOOH/NF, Ir/C/NF, and NF. (b) Required potentials to achieve 100, 500, and 1000 mA·cm^{-2} for NiFeOOH/NF, Ir/C/NF, and $Fe(NO_3)_3$/CP, respectively. (c) Tafel plots for OER over NiFeOOH/NF, Ir/C/NF, and $Fe(NO_3)_3$/CP. (d) Tafel slopes and potentials required for a 100 mA·cm^{-2} comparison of NiFeOOH/NF and other Ni-based OER electrocatalysts (LDH: layered double hydroxide; CN–G: N-doped graphitic carbon). (e) Multicurrent process curve of NiFeOOH/NF. (f) OER LSV curves and durability test after 500 cycles for NiFeOOH/NF (inset: chronopotentiometric curve for NiFeOOH/NF in 1.0 mol·L^{-1} KOH at a current density of 1000 mA·cm^{-2} (without *iR* correction)).

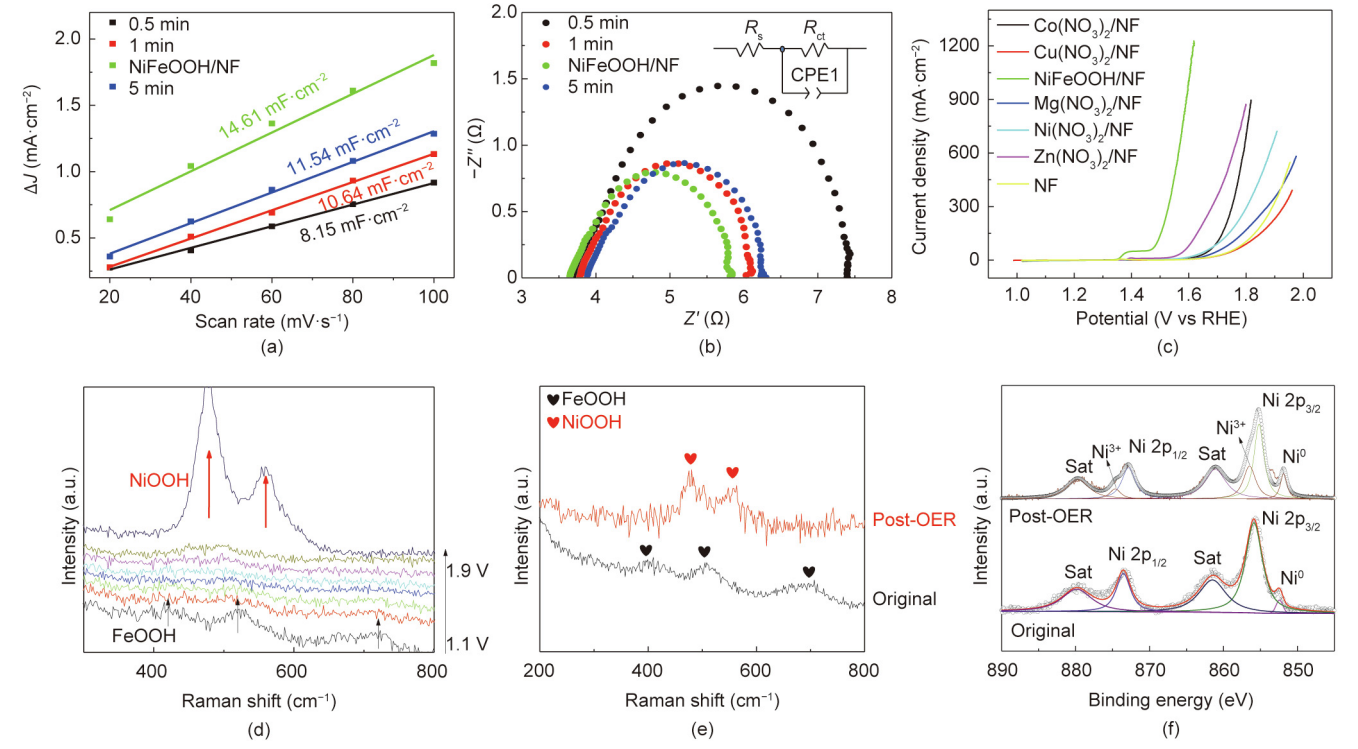

Fig. 3. (a, b) Electrochemical active surface areas (ECSAs) and Nyquist plots of NiFeOOH/NF against the shock time. (c) Polarization curves of $Co(NO_3)_2$/NF, $Cu(NO_3)_2$/NF, NiFeOOH/NF, $Mg(NO_3)_2$/NF, $Ni(NO_3)_2$/NF, $Zn(NO_3)_2$/NF, and NF. (d) Operando Raman spectra of NiFeOOH/NF with different applied potentials. (e) Raman spectra of NiFeOOH/NF before and after OER tests. (f) High-resolution Ni 2p XPS spectra of NiFeOOH/NF before and after the OER test.

results showed that the NiFeOOH/NF hybrid possessed the best OER performance (Fig. 3(c) and Appendix A Fig. S9). In other words, the introduction of the Fe species plays a crucial role in boosting the OER performance, due to the synergistic effect of the Ni and Fe catalytic sites.

In order to evaluate any changes in the composition and structure of the NiFeOOH/NF hybrid throughout the OER operation, *in situ* electrochemical Raman spectroscopy was performed (Fig. 3(d)). At a voltage of 1.1 V, the Raman spectrum presented three main peaks at 422, 520, and 714 cm^{-1} belonging to the FeOOH species. This finding suggests that the active sites were amorphous FeOOH during the initial OER process [2]. As the voltage increased, the peaks of the FeOOH species gradually weakened. When the voltage was increased to 1.5 V, the peaks of the $Ni(OH)_2$ species gradually appeared at 450 and 500 cm^{-1} [25]. With further gradual increase of the voltage, two main peaks at 479 and 560 cm^{-1} were observed, which were attributed to the typical peaks of NiOOH species. Furthermore, the $Ni(OH)_2$ structure was transformed into the compound NiOOH species at a potential of greater than 1.7 V. The Raman spectra of FeOOH and NiOOH before and after the OER process were also compared, and the results were in accord with the *in situ* Raman observations (Fig. 3(e)). Therefore, it can be concluded that the amorphous FeOOH and NiOOH phases in the NiFeOOH/NF hybrid are the actual catalytically active phases, which facilitate the high OER efficiency [40].

To further comprehend the conversion behavior of the NiFeOOH/NF hybrid during the OER operation, the XPS proportions of the NiFeOOH/NF hybrid before and after the OER processes were determined. Compared with the XPS spectra before the OER process (Fig. 3(f)), the high-revolution Ni 2p spectra of the NiFeOOH/NF hybrid after the OER process showed three peaks located at 851.9, 855.2, and 872.8 eV, which were attributed to Ni^0, Ni^{2+} $2p_{3/2}$, and Ni^{2+} $2p_{1/2}$, respectively [41]. Moreover, the two satellite peaks situated at 856.5 and 874.7 eV were ascribed to Ni^{3+} $2p_{3/2}$ and Ni^{3+} $2p_{1/2}$, respectively [31]. These results reveal that transformation of the oxidation states from Ni^{2+} to Ni^{3+} occurred during the OER process; they also confirm that the NiOOH species act as catalytically active centers for the OER.

Along with the high catalytic activity and good stability of the NiFeOOH/NF hybrid, an industry-relevant electrolyte in an operating environment of 10.0 mol·L^{-1} KOH at 80 °C is needed by the OER electrode. As shown in Fig. 4(a), the NiFeOOH/NF hybrid presented ultrahigh current densities of 100, 500, and 1000 mA·cm^{-2} at 1.47, 1.51, and 1.53 V, respectively. Moreover, the NiFeOOH/NF hybrid delivered a current density of up to 3000 mA·cm^{-2} at a low potential of 1.58 V. The NiFeOOH/NF hybrid also exhibited durable stability with a small potential of 1.61 V to achieve 500 mA·cm^{-2} in 10.0 mol·L^{-1} KOH at 80 °C after chronoamperometry testing for over 10 h (Fig. 4(b)). Thus, the NiFeOOH/NF hybrid satisfies the commercial criteria for OER electrocatalysis under harsh industrial conditions. As shown in Fig. 4(c), the NiFeOOH/NF hybrid required the much smaller potentials of 1.51 and 1.53 V to achieve 500 and 1000 mA·cm^{-2} in 10.0 mol·L^{-1} KOH at 80 °C, compared with 1.65 and 1.70 V for $Fe(NO_3)_3$/CP, and 1.73 and 1.80 V for NF, respectively [27]. This simple method was further applied to commercial stainless steel (Figs. 4(d) and (e)) [42]. The $Fe(NO_3)_3$/SUS 304 delivered enhanced electrocatalytic activities as compared with SUS 304, which could be attributed to the displacement reaction of a small amount of Ni species contained in stainless steel with Fe^{3+} in the $Fe(NO_3)_3$ solution. These results demonstrate that the immersion of SUS 304 into $Fe(NO_3)_3$ solution improved the electrocatalytic activity and corrosion resistance of SUS 304 toward the OER process in a basic electrolyte.

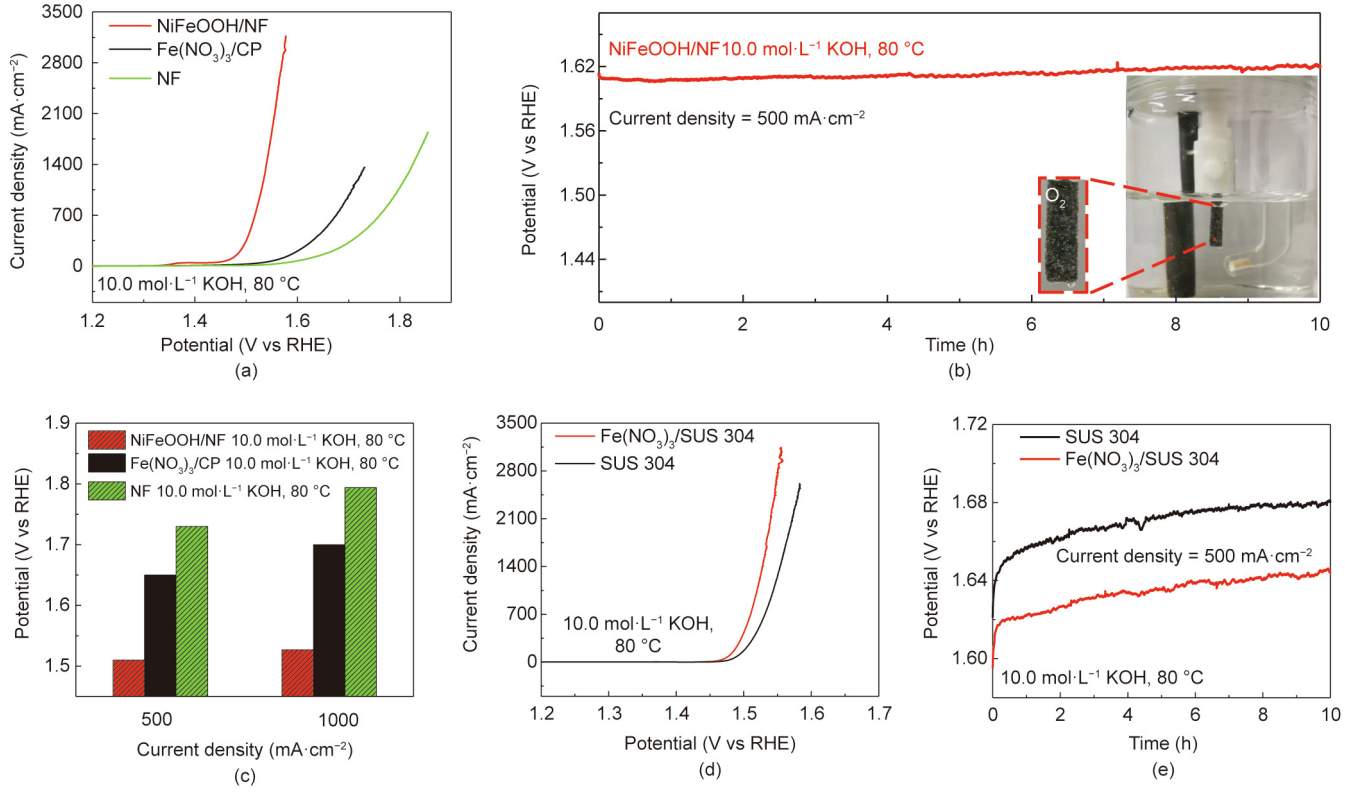

Fig. 4. (a) OER LSV curves of NiFeOOH/NF, $Fe(NO_3)_3$/CP, and NF in 10.0 mol·L^{-1} KOH at 80 °C. (b) Chronopotentiometric curve for NiFeOOH/NF at 500 mA·cm^{-2} (without *iR* correction); inset: image of the O_2 gas evolution on NiFeOOH/NF. (c) Comparison of the potentials required at 500 and 1000 mA·cm^{-2} for NiFeOOH/NF, $Fe(NO_3)_3$/CP, and NF in 10.0 mol·L^{-1} KOH at 80 °C. (d) OER LSV curves of $Fe(NO_3)_3$/SUS 304 and SUS 304 in 10.0 mol·L^{-1} KOH at 80 °C. (e) Chronopotentiometric curves for SUS 304 and $Fe(NO_3)_3$/SUS 304 at 500 mA·cm^{-2} (without *iR* correction), in 10.0 mol·L^{-1} KOH at 80 °C.

4. Conclusions

In conclusion, a novel 3D NiFeOOH/NF hybrid electrocatalyst composed of crystalline $Ni(OH)_2$ and amorphous FeOOH was prepared by means of a simple displacement reaction. The NiFeOOH/NF hybrid showed a strong OER performance, which was evidenced by achieving 500 and 1000 $mA{\cdot}cm^{-2}$ at 1.51 and 1.55 V, respectively, under alkaline conditions. These indicators are superior not only to most reported Ni–Fe-based OER electrocatalysts, but also to the commercial Ir/C catalyst. The achieved OER performance can largely be ascribed to the synergy of the Fe and Ni species. Throughout OER operation, the FeOOH and NiOOH species act as active phases in the NiFeOOH/NF hybrid, as shown by *in situ* electrochemical Raman spectroscopy. In addition, the NiFeOOH/NF hybrid exhibited excellent OER performance under widely adopted harsh electrolyte conditions that are typical for commercial water–alkali electrolyzers. The developed NiFeOOH/NF hybrid introduced here may open an avenue for synthesizing bimetallic oxyhydroxide toward practical applications for clean hydrogen production, along with electrochemical exploration such as CO_2 reduction and O_2 reduction reactions.

Acknowledgements

Y. Hou expresses appreciation for the assistance of the National Natural Science Foundation of China (21922811, 21878270, and 21961160742), the Zhejiang Provincial Natural Science Foundation of China (LR19B060002), the Fundamental Research Funds for the Central Universities (2020XZZX002-09), the Leading Innovative and Entrepreneur Team Introduction Program of Zhejiang (2019R01006), the Startup Foundation for Hundred-Talent Program of Zhejiang University. K. Ostrikov acknowledges partial assistance from the Australian Research Council.

Compliance with ethics guidelines

Jiaxin Yuan, Xiaodi Cheng, Chaojun Lei, Bin Yang, Zhongjian Li, Kun Luo, K.H. Koko Lam, Lecheng Lei, Yang Hou, and Kostya Ken Ostrikov declare that they have no conflict of interest or financial conflicts to disclose.

Appendix A. Supplementary data

Supplementary data to this article can be found online at https://doi.org/10.1016/j.eng.2020.01.018.

References

[1] Zhang J, Zhang Q, Feng X. Support and interface effects in water-splitting electrocatalysts. Adv Mater 2019;31(31):1808167.
[2] Zhou H, Yu F, Zhu Q, Sun J, Qin F, Yu L, et al. Water splitting by electrolysis at high current densities under 1.6 volts. Energy Environ Sci 2018;11(10):2858–64.
[3] Ren JT, Yuan GG, Weng CC, Chen L, Yuan ZY. Uniquely integrated Fe-doped $Ni(OH)_2$ nanosheets for highly efficient oxygen and hydrogen evolution reactions. Nanoscale 2018;10(22):10620–8.
[4] Hou Y, Qiu M, Kim MG, Liu P, Nam G, Zhang T, et al. Atomically dispersed nickel–nitrogen–sulfur species anchored on porous carbon nanosheets for efficient water oxidation. Nat Commun 2019;10(1):1392.
[5] Hou Y, Qiu M, Zhang T, Zhuang X, Kim CS, Yuan C, et al. Ternary porous cobalt phosphoselenide nanosheets: an efficient electrocatalyst for electrocatalytic and photoelectrochemical water splitting. Adv Mater 2017;29(35):1701589.
[6] Lei C, Wang Yu, Hou Y, Liu P, Yang J, Zhang T, et al. Efficient alkaline hydrogen evolution on atomically dispersed Ni–N_x species anchored porous carbon with embedded Ni nanoparticles by accelerating water dissociation kinetics. Energy Environ Sci 2019;12(1):149–56.
[7] Hou Y, Qiu M, Nam G, Kim MG, Zhang T, Liu K, et al. Integrated hierarchical cobalt sulfide/nickel selenide hybrid nanosheets as an efficient three-dimensional electrode for electrochemical and photoelectrochemical water splitting. Nano Lett 2017;17(7):4202–9.
[8] Lei C, Chen H, Cao J, Yang J, Qiu M, Xia Y, et al. Fe–N_4 sites embedded into carbon nanofiber integrated with electrochemically exfoliated graphene for oxygen evolution in acidic medium. Adv Energy Mater 2018;8(26):1801912.
[9] Li M, Tao L, Xiao X, Lv X, Jiang X, Wang M, et al. Core–shell structured $NiCo_2O_4$@FeOOH nanowire arrays as bifunctional electrocatalysts for efficient overall water splitting. Chem Cat Chem 2018;10(18):4119–25.
[10] Babar PT, Lokhande AC, Gang MG, Pawar BS, Pawar SM, Kim JH. Thermally oxidized porous NiO as an efficient oxygen evolution reaction (OER) electrocatalyst for electrochemical water splitting application. J Ind Eng Chem 2018;60:493–7.
[11] Panda C, Menezes PW, Zheng M, Orthmann S, Driess M. *In situ* formation of nanostructured core–shell Cu_3N–CuO to promote alkaline water electrolysis. ACS Energy Lett 2019;4(3):747–54.
[12] Masa J, Sinev I, Mistry H, Ventosa E, de la Mata M, Arbiol J, et al. Ultrathin high surface area nickel boride (Ni_xB) nanosheets as highly efficient electrocatalyst for oxygen evolution. Adv Energy Mater 2017;7(17):1700381.
[13] Hui L, Xue Y, Jia D, Yu H, Zhang C, Li Y. Multifunctional single-crystallized carbonate hydroxides as highly efficient electrocatalyst for full water splitting. Adv Energy Mater 2018;8(20):1800175.
[14] Chi J, Yu H, Qin B, Fu Li, Jia J, Yi B, et al. Vertically aligned FeOOH/NiFe layered double hydroxides electrode for highly efficient oxygen evolution reaction. ACS Appl Mater Interfaces 2017;9(1):464–71.
[15] Chen P, Zhou T, Wang S, Zhang N, Tong Y, Ju H, et al. Dynamic migration of surface fluorine anions on cobalt-based materials to achieve enhanced oxygen evolution catalysis. Angew Chem Int Ed Engl 2018;57(47):15471–5.
[16] Zhang J, Li Y, Zhu T, Wang Y, Cui J, Wu J, et al. 3D coral-like Ni_3S_2 on Ni foam as a bifunctional electrocatalyst for overall water splitting. ACS Appl Mater Interfaces 2018;10(37):31330–9.
[17] Deng Z, Jiang H, Li C. 2D metal chalcogenides incorporated into carbon and their assembly for energy storage applications. Small 2018;14(22):1800148.
[18] Yan Q, Wei T, Wu J, Yang X, Zhu M, Cheng K, et al. Self-supported FeNi–P nanosheets with thin amorphous layers for efficient electrocatalytic water splitting. ACS Sustainable Chem Eng 2018;6(8):9640–8.
[19] Zhang X, Li J, Sun Y, Liu Q, Guo J. Hybridized $Ni(PO_3)_2$–$MnPO_4$ nanosheets array with excellent electrochemical performances for overall water splitting and supercapacitor. Electrochim Acta 2019;299:835–43.
[20] Gong M, Li Y, Wang H, Liang Y, Wu JZ, Zhou J, et al. An advanced Ni–Fe layered double hydroxide electrocatalyst for water oxidation. J Am Chem Soc 2013;135(23):8452–5.
[21] Wu LK, Zhu YX, Liu M, Hou GY, Tang YP, Cao HZ, et al. Ultrafast fabrication of amorphous bimetallic hydroxide layer on nickel nanocones array for oxygen evolution electrocatalyst. Int J Hydrogen Energy 2019;44(12):5899–911.
[22] Alruqi SS, Al-Thabaiti SA, Khan Z. Iron–nickel bimetallic nanoparticles: surfactant assisted synthesis and their catalytic activities. J Mol Liq 2019;282:448–55.
[23] Hou Y, Lohe MR, Zhang J, Liu S, Zhuang X, Feng X. Vertically oriented cobalt selenide/NiFe layered-double-hydroxide nanosheets supported on exfoliated graphene foil: an efficient 3D electrode for overall water splitting. Energy Environ Sci 2016;9(2):478–83.
[24] Cheng X, Pan Z, Lei C, Jin Y, Yang B, Li Z, et al. A strongly coupled 3D ternary Fe_2O_3@Ni_2P/$Ni(PO_3)_2$ hybrid for enhanced electrocatalytic oxygen evolution at ultra-high current densities. J Mater Chem A Mater Energy Sustain 2019;7(3):965–71.
[25] Zhu K, Luo W, Zhu G, Wang J, Zhu Y, Zou Z, et al. Interface-engineered $Ni(OH)_2$/β-like FeOOH electrocatalysts for highly efficient and stable oxygen evolution reaction. Chem Asian J 2017;12(20):2720–6.
[26] Ede SR, Anantharaj S, Kumaran KT, Mishra S, Kundu S. One step synthesis of Ni/$Ni(OH)_2$ nano sheets (NSs) and their application in asymmetric supercapacitors. RSC Adv 2017;7(10):5898–911.
[27] Andronescu C, Seisel S, Wilde P, Barwe S, Masa J, Chen YT, et al. Influence of temperature and electrolyte concentration on the structure and catalytic oxygen evolution activity of nickel–iron layered double hydroxide. Chemistry 2018;24(52):13773–7.
[28] Chi JQ, Shang X, Liang F, Dong B, Li X, Liu YR, et al. Facile synthesis of pyrite-type binary nickel iron diselenides as efficient electrocatalyst for oxygen evolution reaction. Appl Surf Sci 2017;401:17–24.
[29] Zhou P, He J, Zou Y, Wang Y, Xie C, Chen Ru, et al. Single-crystalline layered double hydroxides with rich defects and hierarchical structure by mild reduction for enhancing the oxygen evolution reaction. Sci China Chem 2019;62(10):1365–70.
[30] Liu H, Lu X, Hu Yi, Chen R, Zhao P, Wang L, et al. Co_xFe_yN nanoparticles decorated on graphene sheets as high-performance electrocatalysts for the oxygen evolution reaction. J Mater Chem A Mater Energy Sustain 2019;7(20):12489–97.
[31] Liu Z, Yu H, Dong B, Yu X, Feng L. Electrochemical oxygen evolution reaction efficiently boosted by thermal-driving core–shell structure formation in nanostructured FeNi/S, N-doped carbon hybrid catalyst. Nanoscale 2018;10(35):16911–8.
[32] Ma L, Zhang W, Zhao P, Liang J, Hu Y, Zhu G, et al. Highly efficient overall water splitting driven by all-inorganic perovskite solar cells and promoted by bifunctional bimetallic phosphide nanowire arrays. J Mater Chem A Mater Energy Sustain 2018;6(41):20076–82.
[33] Liu H, Wang Y, Lu X, Hu Y, Zhu G, Chen R, et al. The effects of Al substitution and partial dissolution on ultrathin NiFeAl trinary layered double hydroxide nanosheets for oxygen evolution reaction in alkaline solution. Nano Energy 2017;35:350–7.

[34] Ma L, Hu Y, Chen R, Zhu G, Chen T, Lv H, et al. Self-assembled ultrathin $NiCo_2S_4$ nanoflakes grown on Ni foam as high-performance flexible electrodes for hydrogen evolution reaction in alkaline solution. Nano Energy 2016;24:139–47.
[35] Yin H, Jiang L, Liu P, Al-Mamun M, Wang Y, Zhong YL, et al. Remarkably enhanced water splitting activity of nickel foam due to simple immersion in a ferric nitrate solution. Nano Res 2018;11(8):3959–71.
[36] Zhu Y, Zhou W, Zhong Y, Bu Y, Chen X, Zhong Q, et al. A perovskite nanorod as bifunctional electrocatalyst for overall water splitting. Adv Energy Mater 2017;7(8):1602122.
[37] Zou Y, Liu Z, Liu R, Liu D, Dong C, Wang Y, et al. Disordered CoFePi nanosheets with rich vacancies as oxygen evolving electrocatalysts: insight into the local atomic environment. J Power Sources 2019;427:215–22.
[38] Xu L, Zou Y, Xiao Z, Wang S. Transforming Co_3O_4 nanosheets into porous N-doped Co_xO_y nanosheets with oxygen vacancies for the oxygen evolution reaction. J Energy Chem 2019;35:24–9.
[39] Ye Z, Qin C, Ma G, Peng X, Li T, Li D, et al. Cobalt–iron oxide nanoarrays supported on carbon fiber paper with high stability for electrochemical oxygen evolution at large current densities. ACS Appl Mater Interfaces 2018;10(46):39809–18.
[40] Zhu K, Zhu X, Yang W. Application of *in situ* techniques for the characterization of NiFe-based oxygen evolution reaction (OER) electrocatalysts. Angew Chem Int Ed Engl 2019;58(5):1252–65.
[41] Tang Yi, Yang C, Yang Y, Yin X, Que W, Zhu J. Three dimensional hierarchical network structure of S-$NiFe_2O_4$ modified few-layer titanium carbides (MXene) flakes on nickel foam as a high efficient electrocatalyst for oxygen evolution. Electrochim Acta 2019;296:762–70.
[42] Guo F, Wu Y, Chen H, Liu Y, Yang L, Ai X, et al. High-performance oxygen evolution electrocatalysis by boronized metal sheets with self-functionalized surfaces. Energy Environ Sci 2019;12(2):684–92.